Available online at www.sciencedirect.com

ScienceDirect

IFAC PapersOnline CONFERENCE PAPER ARCHIVE

IFAC PapersOnLine 55-12 (2022) 402–407

Adaptive Learning for Maximum Takeoff Efficiency of High-Speed Sailboats

Renato Rodriguez * **Yan Wang** ** **Jozeph Ozanne** ***
Dogan Sumer** **Dimitar Filev**** **Damoon Soudbakhsh***

* *Dynamical Systems Lab (DSLab), Temple University, Philadelphia, PA, USA (e-mail: damoon.soudbakhsh@temple.edu),*
** *Ford Motor Company, Dearborn, MI, USA,*
*** *American Magic, New York Yacht Club, USA.*

Abstract: This paper presents an optimal takeoff maneuver for an AC75 foiling sailboat competing in the America's Cup. The innovative sailboat design introduces extra degrees of freedom and articulations in the boat that result in nonlinear, high-dimensional, and unstable dynamics. The optimal maneuvers were achieved by exploring out-of-the-box solutions through adaptive control and optimization. We used a high-fidelity sailboat simulator for the data generation process and an adaptive control approach (Jacobian Learning (JL)) to optimize the sailing maneuver. Takeoff is a dynamic sailboat maneuver that involves transitioning the boat from a low-speed in-water status (displacement mode) to a high-speed out-of-water status (foiling mode) via actuation of the sailboat's inputs. We optimized the time for the boat's transitions from displacement mode to foiling mode while maximizing the projection of the velocity (Velocity Made Good (VMG)) in the desired target direction (True Wind Angle (TWA)). Furthermore, we optimized the sailboat's upwind steady-state performance (closed-haul VMG) for varying sailing directions (TWA) and used the optimal TWA to formulate the takeoff. The optimal solution is subject to physical/actuator constraints and the ones enforced to ensure the feasibility of the maneuvers by humans (sailors). The optimal takeoff achieved an average VMG of 7.42 m/s. This maneuver serves as a performance benchmark for the sailors and provides insightful information about the underlying dynamics of the boat.

Copyright © 2022 The Authors. This is an open access article under the CC BY-NC-ND license (https://creativecommons.org/licenses/by-nc-nd/4.0/)

Keywords: Identification for control, Adaptive control -applications, Surface vehicles, Jacobian Learning, Iterative learning control.

1. INTRODUCTION

This paper presents an adaptive learning and control approach to maximize the takeoff efficiency of an AC75 sailboat. Sailing has been used throughout history to aid and promote the development of the human race. It has been widely applied to many fields such as fishing, trade, and exploration. In modern times, sailing is also commonly used for sporting events, like America's Cup. America's Cup is the oldest, most prestigious, and technologically advanced sailing race. During every installment, new and innovative sailboat designs are introduced to improve sailing performance. However, these radical designs also result in greater complexity in the control of the system (Bencatel et al., 2020; Rodriguez et al., 2022). The AC75 sailboat has nonlinear, high-dimensional, and unstable dynamics with switching operational modes, including displacement mode, where the hull is in contact with the water, and foiling mode, where the hull travels above the waterline (Bencatel et al., 2020). Such complex cost topologies make analytical maneuver optimization computationally prohibitive using a traditional model-based approach. This study implements an adaptive learning approach known as Jacobian Learning to develop a maximum efficiency takeoff maneuver for the multi-input multi-output (MIMO) AC75 sailboat. The optimal solution yields insight into the system's complex underlying dynamics and sets a performance benchmark for the sailors.

Table 1. Nautical Terminology

Term	Definition
surge (x, u)	(position,velocity) along the longitudinal axis
sway (y, v)	(position,velocity) along the lateral axis
heave (z, w)	(position,velocity) along the vertical axis
roll (ϕ, p)	(angle, angular rate) about longitudinal axis
pitch (θ, q)	(angle, angular rate) about lateral axis
yaw (ψ, r)	(angle, angular rate) about vertical axis
Hull	sailboat body
Rudder	heading (TWA) input
Rudder Rake	pitch input
Cants	canting hydrofoil input
Flaps	ride-height input
Traveler	roll input
Displacement	sailing with the hull in contact with the water
Foiling	sailing with the hull above the waterline
TWS	True wind speed (environmental parameter)
TWA	True wind angle (akin to heading angle)
VMG	Velocity-made-good

* From Rodriguez (2021)

Modeling and control of aquatic vehicles have been an active area of research over the last few decades. Studies

2405-8963 Copyright © 2022 The Authors. This is an open access article under the CC BY-NC-ND license.
Peer review under responsibility of International Federation of Automatic Control.
10.1016/j.ifacol.2022.07.345

in this field include topics such as exploring the design space (Gale and Walls, 2000; Furrer and Siegwart, 2010; Heppel, 2015; Bousquet et al., 2017; Horel et al., 2019; Horel, 2019), trajectory control (Sclavounos and Borgen, 2004; Le Bars and Jaulin, 2013; Xiao and Jouffroy, 2013; Alves and Cruz, 2015; Melin et al., 2015; Wang et al., 2017; Abrougui et al., 2019; Rodriguez and Soudbakhsh, 2019), and maneuver optimization (Ren and Yang, 2004; Skjetne et al., 2004; Xiao et al., 2012; Corno et al., 2015; Sun et al., 2018; dos Santos and Goncalves, 2019; da Silva Junior et al., 2020; Bencatel et al., 2020).

For traditional sailboats, simplified three degrees of freedom (DOF) and 4-DOF models are often used for trajectory control (Xiao and Jouffroy, 2013) and maneuver optimization (Xiao et al., 2012). However, such models are not applicable to the AC75 sailboat, which requires the inclusion of all 6-DOF (Heppel, 2015; Horel, 2019; Horel et al., 2019; Zheng et al., 2021) due to its complex and switching dynamical behavior. This complex behavior is experienced when the position of the articulating hydrofoil arms (Cants) is changed during the turning maneuvers or when the boat switches between its different operational modes, changing its underlying dynamics (Horel et al., 2019). This requires an accurate representation of the interaction between the water and the hydrofoils (fluid-structure interaction (FSI)) and characterization of the transient response of the system along the 6-DOFs (Horel, 2019; Horel et al., 2019). The state variables for a 6-DOF model with motion along the surge, sway, heave, yaw, pitch, and roll DOFs are:

$$\text{Body Frame: } \nu = [u \ v \ w \ p \ q \ r] \tag{1}$$

$$\text{Global Frame: } \eta = [X \ Y \ Z \ \phi \ \theta \ \psi]\,. \tag{2}$$

We seek the optimal takeoff maneuver utilizing an adaptive learning scheme (Filev et al., 1999; D'Amato et al., 2017) that involves learning the system's Jacobian and adjusting the control input. This approach is not limited to reduced-order modeling. Hence, the optimized inputs are valid for the complex dynamics of the AC75 sailboat. These optimal maneuvers are achieved using a high-fidelity simulator that models the highly nonlinear and high-dimensional dynamics of the sailboat, as well as the articulations in the boat. The contributions of this research are adaptive learning for switching dynamics of an open-loop unstable system. We optimized the maneuver and control inputs of an AC75 sailboat for a fast takeoff maneuver while maximizing speed in the desired direction of travel (i.e., VMG). The maneuvers were subject to physical constraints as well as operational constraints (due to the sailors' abilities).

2. SYSTEM DESCRIPTION AND ANALYSIS

The system of interest for this research is the AC75 foiling sailboat designed and developed by the New York Yacht Club American Magic (AM) sailing team. This system is complex, with nonlinear, high-dimensional, and unstable dynamics. This system undergoes several operational modes, including displacement and foiling modes, where substantial improvements to the sailing performance are expected due to the reduction of wetted surfaces affected by hydrodynamic drag. However, such improvements result in higher complexities in the control of the sailboat system (Bencatel et al., 2020).

Table 2. Physical and Operational Constraints

Parameters	**Constraints**
Rudder Angle [deg]	$[-30, 30]$
Rudder Rate [deg/s]	$[-5, 5]$
Rudder-Rake Angle [deg]	$[-3, 7]$
Flap Angle [deg]	$[-8, 10]$
Cant Angle [deg]	$[10, 80]$
Cant Rate [deg/s]	[down, up]: $[-60, 40]$
Ride-height [m]	$RH > 0$ (above waterline)
Pitch [deg]	$[-3, 3]$
Roll [deg]	$[-3, 3]$
Rudder-Rake Rate [deg/s]	$[-2, 2]$

* From Rodriguez (2021)

Here we aim at maximizing the performance achieved by the optimal maneuvers by optimizing the sailboat speed and its projection onto the wind direction, VMG (refer to §2.2).

The optimizations are performed on a high-fidelity AC75-sailboat simulator developed by AM. However, these maneuvers should be performed by the human sailors; therefore, we consider the constraints due to the sailors' abilities and the physical constraints.

2.1 Simulator

The simulator was developed by AM for input-output data generation of the AC75 sailboat and was validated with extensive simulations and real-world sailing. It provides an accurate model of the foiling sailboat's motion along all 6-DOFs (and the mechanisms). It provides a platform for efficient design and testing out-of-the-box sailing maneuvers and strategies in a safe and controlled environment. Furthermore, the simulator allows for implementing data-driven/adaptive control schemes for maneuver optimization.

System Parameters and Constraints The simulator provides access to kinematic, dynamic, and environmental (i.e., wind speed) data via its various parameters. The main control inputs include the rudder, rudder-rake, traveler, Cants, and flaps while the outputs include the true wind angle (TWA), pitch angle, roll angle, ride height, surge speed (u), and the windward projection of the sailboat's speed (VMG). These variables are subject to value and rate constraints based on the physical limitations of the actuators as well as the sailors' abilities to perform the sailing maneuvers in a real-world scenario (operational constraints), refer to Table 2.

2.2 Optimization Criteria

The race starts with the sailboat in displacement mode, where the hull is in contact with the water. Here the sailboat experiences significant drag on the wetted surfaces, including the hull and hydrofoils, resulting in stunted performance. To enhance the performance and maneuverability of the sailboat, hydrofoils (cants, flaps) are used to provide active lift control, allowing the system to perform the takeoff maneuver and lift the boat above the waterline and into foiling mode. After achieving foiling status, the boat is on an upwind course.

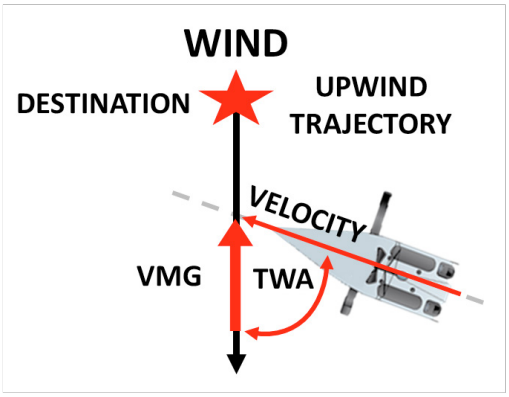

Fig. 1. Depiction of sailing metrics for an upwind trajectory

We optimized the time for the boat's transitions from displacement mode to foiling mode by optimizing its speed profile to decrease the overall drag experienced throughout the maneuver. The optimization criteria include VMG and completion of the maneuver in minimum time. The relationship between the sailboat's heading (TWA), and the performance metric (VMG) is shown in Fig. 1 and is given by:

$$\text{VMG} = \text{Speed} \cdot \cos(\text{TWA}). \tag{3}$$

3. ADAPTIVE LEARNING OPTIMIZATION

This section summarizes the data generation process in §3.1 and the methodology of the adaptive control approach (Jacobian learning)in §3.2.

3.1 Data-Generation/Exploratory Data Analysis

The maneuver optimization problem was tackled via an adaptive learning approach that requires the generation of input-output data. The data is generated by perturbing a baseline set of input signals and assessing the system's response around this known working point (input-output mapping). To allow for simple and accurate mappings, a signal parameterization is performed on the dynamic signals (i.e., rudder) and the switching signals (i.e., cants).

3.2 Jacobian learning with Gradient-based Optimization

This adaptive learning optimization (Jacobian Learning (JL)) utilizes learning methods to identify and recursively update the input/output sensitivity of the system and is used to control the MIMO AC75 sailboat. Refer to Table 3 for a description of the nomenclature used for the JL method.

Problem Formulation The Jacobian Learning approach considers zero-order systems, represented by:

$$y[k] = S(u[k]), \tag{4}$$

where S is a smooth nonlinear mapping between the system's inputs $u[k]$ and outputs $y[k]$. We seek a control law that minimizes the tracking error $e[k]$:

$$e[k] = (y[k] - y_d)^T (y[k] - y_d) \tag{5}$$

To achieve this goal, inversion of the mapping operator of (6) is needed. Due to measurement noise and model uncertainties, however, direct inversion of S can lead to numerical errors. Hence, a Kalman filter is used with JL to account for measurement noise via the variance R_j and covariance Q_j parameters.

Table 3. Nomenclature for Jacobian Learning

Term	Definition
$u[k]$	discrete-time representation of the input vector $\mathbf{u}$
$y[k]$	discrete-time representation of the output vector $\mathbf{y}$
y_d	Target Output
$e[k]$	Error between measured output and target
$\hat{\mathbb{J}}[k]$	discrete-time representation of the learned Jacobian $\hat{\mathbb{J}}$
r	Number of control inputs
q	Number of measured outputs
$w_j[k]$	Variability in the linearized model
$v_j[k]$	Measurement noise
Q_j	Covariance of the linear model's imprecision $w_j[k]$
R_j	Variance of the measurement noise $v_j[k]$
$P_j[k]$	Covariance of Kalman filter that controls learning rate

* From Rodriguez (2021)

The nonlinear mapping is approximated via a linearized time-varying representation given by:

$$\Delta \mathrm{y}[k] = \mathbb{J}[k]\ \Delta \mathrm{u}[k], \tag{6}$$

where the change in input $\Delta u[k]$, output $\Delta y[k]$ and Jacobian are given by:

$$\Delta u[k] = u[k] - u[k-1], \qquad \Delta u[k] \epsilon \mathbb{R}^r, \tag{7}$$

$$\Delta y[k] = y[k] - y[k-1], \qquad \Delta y[k] \epsilon \mathbb{R}^q, \tag{8}$$

$$\Delta \mathbb{J}[k] = \left(\frac{\partial y_s[k]}{\partial u_j[k]} \right), \tag{9}$$

with $j \in 1, 2, .., q$ and $s \in 1, 2, ..., r$, and $\mathbb{J}$ denotes the linearized Jacobian matrix about the working point $(u[k], y[k])$.

The Kalman filter was used to learn and recursively update the Jacobian. It is implemented by decomposing the linearized MIMO system (6) into q multi-input single-output (MISO) subsystems. Here we assume that while the plant (S) evolves with time, the Jacobian in the linearized representation evolves with $u[k]$ due to the plant's nonlinear behavior. Thus, the piece-wise linearized plant dynamics where each subsystem maps all the inputs to one output is given by:

$$\Delta y_j[k] = \mathbb{J}_j^T[k] \Delta u[k], \tag{10}$$

where $\mathbb{J}_j^T$ is the j^{th} row of the Jacobian $\mathbb{J}$. Next, we use (11)-(12) to approximate the Jacobian's evolution in time

$$\mathbb{J}_j[k+1] = \mathbb{J}[k] + w_j[k], \tag{11}$$

$$\Delta y_j[k] = \Delta u^T[k] \mathbb{J}_j[k] + v_j[k], \quad j \in [1, q], \tag{12}$$

where the vector $w_j[k]$ denotes the model uncertainty and $v_j[k]$ represents the measurement noise.

To achieve a recursive update of the learned Jacobian matrix $\hat{\mathbb{J}}_j$, a Kalman filter is implemented to the MISO subsystems resulting in the following representation:

$$\hat{\mathbb{J}}_j^T[k] = \hat{\mathbb{J}}_j^T[k-1] + \frac{P_j[k-1]\Delta u[k](\Delta y[k] - \hat{\mathbb{J}}_j[k-1]\Delta u[k])}{R_j + \Delta u^T[k] P_j[k-1] \Delta u[k]}, \tag{13}$$

$$P_j[k] = P_j[k-1] - \frac{P_j[k-1]\Delta \mathrm{u}[k]\Delta u^T[k] P_j[k-1]}{R_j + \Delta u^T[k] P_j[k-1] \Delta u[k]} + Q_j, \tag{14}$$

where Q_j represents the drift/forgetting factor and is estimated using $Q_j = E\{w_j^T[k]w_j[k]\}$, and $R_i = E\{v_i^2[k]\}$ is the measurement noise variance $v_i[k]$. We note that the Kalman filter's covariance matrix, $P_j[k]$, controls the learning rate, and the drift factor, Q_j, ensures linear growth of $P_j[k]$, when the system is not excited.

The next step in the process is to integrate the Jacobian Learning algorithm into the control problem and simultaneously determine the optimal control inputs. For a MIMO system with unknown dynamics this is achieved using the following constrained optimization problem (Filev et al., 2000):

$$u[k] = \underset{u[k]\in U}{\arg\min}(\|y_d - \hat{y}[k]\|_2^2 + \alpha \|u[k] - u[k-1]\|_2^2) \quad (15)$$
$$\text{with} \qquad \hat{y}[k] = y[k-1] + \hat{\mathbb{J}}(u[k] - u[k-1]).$$

This problem can be tackled via different optimization routines, such as MATLAB's LSQLIN (constrained linear least-squares) solver. This solver-based approach allows for developing optimization schemes that actively compute the constrained Jacobian-based optimal control laws which drive the error to zero in the presence of unknown disturbances (Rodriguez, 2021). The adaptive Jacobian learning approach was used for offline constrained optimization of the VMG performance metric subject to the control constraints detailed in §2.1.1.

4. RESULTS

This section presents the optimization results for close-hauled (upwind steady-state) sailing in §4.1 and the takeoff maneuver in §4.2. These optimizations were performed for various environmental conditions, including different heading angles (TWA) at wind speeds of 15 [knots] (7.166 $[m/s]$).

4.1 Close-Hauled

The close-hauled segment involves steady-state (SS) straight-line sailing in a windward direction. To achieve this, the vehicle must sail at an angle (TWA) relative to the wind direction to avoid loss of propulsive power, which occurs when sailing directly into the wind. Thus, closed-haul sailing includes both windward and lateral (left/right) motions.

Closed-haul optimizations were performed for TWAs (heading angles) in the range of 35° to 60°. A comparison of the results is presented in the form of a polar plot, Fig. 2a, which depicts a graph of vehicle speed across varying TWAs. Using the relationship between the speed and TWA given in (3), the respective VMG (windward projection of the speed) for each TWA is found. Fig. 2b presents the average VMG results across the TWA range. TWA of 45° (TWA45) yielded the best sailing performance (SS-VMG) and SS surge velocity of 11.74 m/s and 16.60 m/s, respectively. This was achieved utilizing the optimized Cant (articulating hydrofoil-arm), flap (lifting hydrofoil/ride-height input), and traveler (roll input) angles. The position of the IW (in-water/submerged) flap and traveler were kept near their neutral positions (0°), indicating that the boat is relatively stable since they are not working to compensate for disparities in the ride

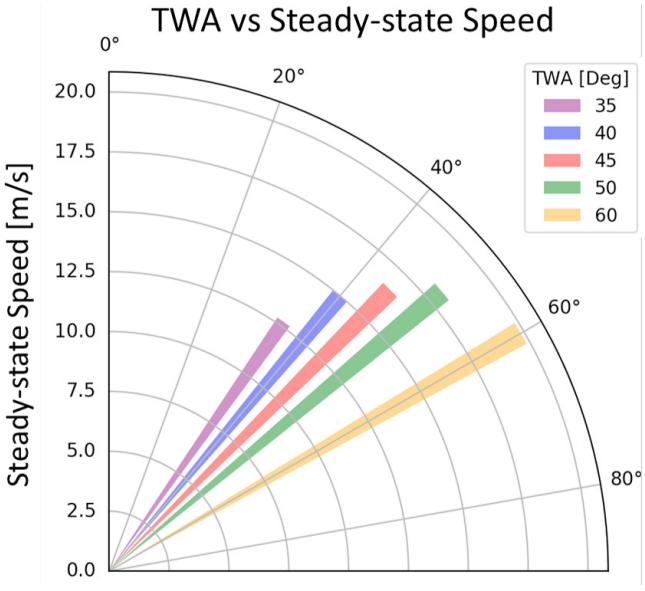

(a) Polar plot

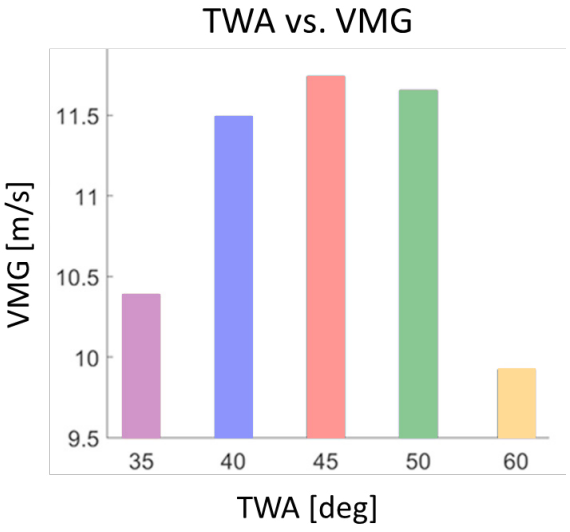

(b) Optimal VMG

Fig. 2. Optimization results for closed-haul sailing: (a) Optimal Polar plot, and (b) Optimal VMG

height or heel. Table 4 shows the optimized parameters for each TWA corresponding to close-hauled. Note that close-hauled sailing follows the takeoff maneuver. Thus, the optimal TWA of 45° is used as the final targeted direction for the takeoff.

4.2 Takeoff

The race starts with the sailboat in displacement mode with the hull in contact with the water (negative ride-height) and with a low boat speed. The overall objective of the takeoff maneuver is to transition the boat from displacement mode to foiling mode, where the hull is above the waterline. Additionally, once the foiling status is achieved, a transition (heading change) to a heading (TWA) of 45° is needed to set up for closed-haul sailing. The takeoff maneuver is deemed finished when a steady-state (SS) heading and SS-VMG are reached.

Table 4. Optimal parameters for Close-Hauled sailing

TWA [deg]	SS Speed $[m/s]$	SS VMG $[m/s]$	IW Flap [deg]	IW Cant [deg]	Traveler [deg]	Rudder-Rake [deg]
35	12.70	10.41	0.101	24.4	0.196	2.69
40	14.98	11.52	2.01	23.8	2.67	3.57
45	16.60	11.74	-0.60	23.8	2.17	3.36
50	18.14	11.66	-1.18	26	2.87	2.94
60	19.85	9.93	-2.48	23.8	2.795	2.89

The first part of the takeoff happens when the boat's speed reaches 17 [knots] (8.745 $[m/s]$). At this point, the lift induced on the flap raises the boat above the waterline (positive ride height), yielding significant improvements in sailing speed and maneuverability. The final step includes maneuvering the boat to the targeted direction (TWA45) via actuation of the rudder input and reaching the corresponding SS Cant and SS flap angles (refer to Tab: 4).

The optimal inputs and outputs of the takeoff maneuver are presented in Fig. 3 and Fig. 4, respectively. This maneuver implements dynamic signals for inputs such as the rudder and flap and switching signals for the rudder-rake and Cant, and includes system outputs such as TWA, pitch, ride height, and VMG. The flap (lifting hydrofoil/pitch-input) signal includes an initially sloped profile tuned to provide maximum acceleration while in displacement mode. This is achieved by generating a high initial lifting force due to the use of a high flap angle. However, as the signal evolves in time, the flap angle gradually decreases, allowing for a balance between lift and drag induced on the flap to be considered. Similarly, the rudder-rake (pitch-input) signal was tuned via a switching perturbation from the nominal value. This perturbation was applied just before the boat reached the takeoff velocity of 17 [knots], resulting in an increase in pitch that acted as a 'jump-start' to the takeoff process by providing an extra lifting force critical point in the maneuver. We note that these perturbations are short enough in duration that no resulting instability occurs. Implementing these highly tuned input signals allowed the system to transition from displacement mode into foiling mode, where the effects of drag are drastically reduced, in minimum time, thus, resulting in optimal sailing performance (VMG). The optimal takeoff maneuver achieved an average VMG of 7.42 [m/ s] and completed the entire maneuver in 36.4 [s].

We note that the stability and robustness of the adaptive control laws developed in this research were assessed via several sensitivity studies performed with small deviations from the optimal angles and wind speeds.

5. CONCLUSION

In this research, an optimal takeoff maneuver was developed for an AC75 sailboat racing in America's Cup. This system has complex dynamics due to its various operational modes, including displacement and foiling. The optimal maneuvers were developed using an Adaptive (Jacobian Learning) optimization approach and input-output data from a high-fidelity sailboat simulator. The optimization process focused on completing the takeoff maneuver in minimum time via optimization of the boat's speed profile along with its projection onto the wind direction (VMG).

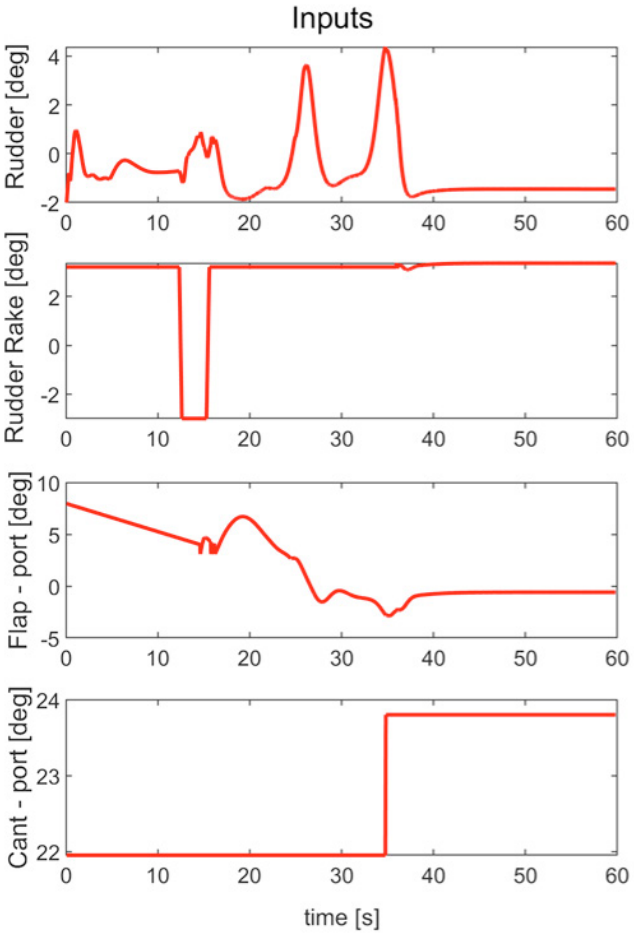

Fig. 3. Optimal inputs of the takeoff maneuver

The optimal takeoff maneuver achieved an average VMG of 7.42 [m/s] and completed the entire maneuver in 36.4 [s]. The optimal solution is subject to physical constraints and the ones enforced to ensure the feasibility of the maneuvers by humans (sailors). Furthermore, the maneuvers developed in this research provide insightful information about the complex underlying dynamics of this foiling sailboat and serve as performance benchmarks for the sailors.

REFERENCES

Abrougui, H., Dallagi, H., and Nejim, S. (2019). Autopilot design for an autonomous sailboat based on sliding mode control. *Automatic Control and Computer Sciences*, 53(5), 393–407.

Alves, J.C. and Cruz, N.A. (2015). Ais-enabled collision avoidance strategies for autonomous sailboats. In *World Robotic Sailing championship and International Robotic Sailing Conference*, 77–87. Springer.

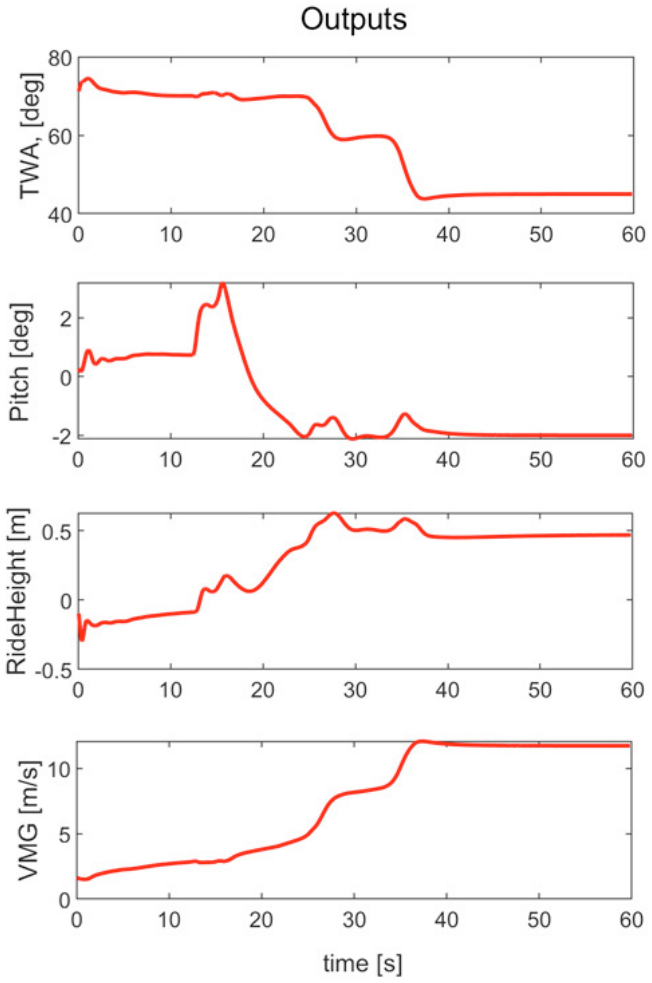

Fig. 4. Optimal outputs of the takeoff maneuver

Bencatel, R., Keerthivarman, S., Kolmanovsky, I., and Girard, A.R. (2020). Full state feedback foiling control for america's cup catamarans. *IEEE TCST*, 29(1), 1–17.

Bousquet, G.D., Triantafyllou, M.S., and Slotine, J.J.E. (2017). Control of a flexible, surface-piercing hydrofoil for high-speed, small-scale applications. In *IROS'17*, 4203–4208.

Corno, M., Formentin, S., and Savaresi, S.M. (2015). Data-driven online speed optimization in autonomous sailboats. *IEEE trans. ITS*, 17(3), 762–771.

da Silva Junior, A.G., Dos Santos, D.H., de Negreiros, A.P.F., de Souza, J.M.V.B., et al. (2020). High-level path planning for an autonomous sailboat robot using q-learning. *Sensors (Basel, Switzerland)*, 20(6).

D'Amato, A., Wang, Y., Filev, D., and Remes, E. (2017). On the Tradeoffs between Static and Dynamic Adaptive Optimization for an Automotive Application. *SAE International Journal of Commercial Vehicles*, 10(1), 346–352.

dos Santos, D.H. and Goncalves, L.M.G. (2019). A gain-scheduling control strategy and short-term path optimization with genetic algorithm for autonomous navigation of a sailboat robot. *IJARS*, 16(1), 1729881418821830.

Filev, D., Larsson, T., and Ma, L. (2000). Intelligent control for automotive manufacturing-rule based guided adaptation. In *26th IECON*, volume 1, 283–288.

Filev, D.P., Bharitkar, S., and Tsai, M.F. (1999). Nonlinear control of static systems with unsupervised learning of the initial conditions. In *18th NAFIPS (Cat. No. 99TH8397)*, 169–173.

Furrer, F. and Siegwart, R. (2010). Developing a simulation model of a catamaran using the concept of hydrofoils. *ETH Zurich*.

Gale, T. and Walls, J. (2000). Development of a sailing dinghy simulator. *Simulation*, 74(3), 167–179.

Heppel, P. (2015). Flight dynamics of sailing foilers. In *5th HPYD*, volume 12.

Horel, B. (2019). System-based modelling of a foiling catamaran. *Ocean Engineering*, 171, 108–119.

Horel, B., Durand, M., et al. (2019). Application of system-based modelling and simplified-fsi to a foiling open 60 monohull. *Journal of Sailing Technology*, 4(1), 114–141.

Le Bars, F. and Jaulin, L. (2013). An experimental validation of a robust controller with the vaimos autonomous sailboat. In *Robotic Sailing 2012*, 73–84. Springer.

Melin, J., Dahl, K., and Waller, M. (2015). Modeling and control for an autonomous sailboat: a case study. In *WRSC & IRSC*, 137–149. Springer.

Ren, J. and Yang, Y. (2004). Fuzzy gain scheduling attitude control for hydrofoil catamaran. In *2004 ACC*, volume 2, 1103–1108.

Rodriguez, R. (2021). *Optimal Control of the AC75 sailboat for the America's cup race*. Master's thesis, Temple University. Libraries.

Rodriguez, R. and Soudbakhsh, D. (2019). Modeling and predictive control of an unmanned underwater vehicle. In *2019 DSCC*, volume 59162.

Rodriguez, R., Wang, Y., Ozanne, J., Sumer, D., Filev, D., and Soudbakhsh, D. (2022). Adaptive Takeoff Maneuver Optimization of a Sailing Boat for America's Cup. *Journal of Sailing Technology (in-Press)*.

Sclavounos, P.D. and Borgen, H. (2004). Seakeeping analysis of a high-speed monohull with a motion-control bow hydrofoil. *Journal of Ship Research*, 48(02), 77–117.

Skjetne, R., Fossen, T.I., and Kokotović, P.V. (2004). Robust output maneuvering for a class of nonlinear systems. *Automatica*, 40(3), 373–383.

Sun, Q., Qiao, Z., Strömbeck, C., Qu, Y., Liu, H., and Qian, H. (2018). Tacking control of an autonomous sailboat based on force polar diagram. In *13th WCICA*, 467–473. IEEE.

Wang, N., Su, S.F., Yin, J., Zheng, Z., and Er, M.J. (2017). Global asymptotic model-free trajectory-independent tracking control of an uncertain marine vehicle: An adaptive universe-based fuzzy control approach. *IEEE TFS*, 26(3), 1613–1625.

Xiao, L., Alves, J.C., Cruz, N.A., and Jouffroy, J. (2012). Online speed optimization for sailing yachts using extremum seeking. In *2012 Oceans*, 1–6. IEEE.

Xiao, L. and Jouffroy, J. (2013). Modeling and nonlinear heading control of sailing yachts. *IEEE J. Ocean. Eng*, 39(2), 256–268.

Zheng, L., Liu, Z., Li, G., Yuan, S., and Yang, S. (2021). Experimental and numerical investigation on control strategies for heave and pitch motion reduction of a catamaran. *Proceedings of the Institution of Mechanical Engineers, Part M: Journal of Engineering for the Maritime Environment*, 235(2), 311–326.